JACS
JOURNAL OF THE AMERICAN CHEMICAL SOCIETY

Article

Binding of the bacterial adhesin FimH to its natural, multivalent high-mannose type glycan targets

Maximilian M. Sauer, Roman P. Jakob, Thomas Luber, Fabia Canonica, Giulio Navarra, Beat Ernst, Carlo Unverzagt, Timm Maier, and Rudi Glockshuber

J. Am. Chem. Soc., **Just Accepted Manuscript** • DOI: 10.1021/jacs.8b10736 • Publication Date (Web): 13 Dec 2018

Just Accepted

ACS Publications

is published by the American Chemical Society. 1155 Sixteenth Street N.W., Washington, DC 20036

Binding of the bacterial adhesin FimH to its natural, multivalent high-mannose type glycan targets

Maximilian M. Sauer[†], Roman P. Jakob[‡], Thomas Luber[§], Fabia Canonica[†], Giulio Navarra[¶], Beat Ernst[¶], Carlo Unverzagt[§], Timm Maier[‡], Rudi Glockshuber[*,†]

[†]Institute of Molecular Biology & Biophysics, ETH Zurich, Otto-Stern-Weg 5, CH-8093 Zurich, Switzerland

[‡]Biozentrum, University of Basel, Klingelbergstrasse 50/70, CH-4056 Basel, Switzerland

[§]Bioorganische Chemie, University of Bayreuth, D-95440 Bayreuth, Germany

[¶]Department of Pharmaceutical Sciences, University of Basel, Klingelbergstrasse 50, CH-4056 Basel, Switzerland

*Corresponding author:

Rudi Glockshuber

Institute of Molecular Biology & Biophysics

ETH Zurich

Otto-Stern-Weg 5

CH-8093 Zurich

Switzerland

E-mail: rudi@mol.biol.ethz.ch

Phone: +41-44-6336819

ABSTRACT

Multivalent carbohydrate-lectin interactions at host-pathogen interfaces play a crucial role in the establishment of infections. Although competitive antagonists that prevent pathogen adhesion are promising anti-microbial drugs, the molecular mechanisms underlying these complex adhesion processes are still poorly understood. Here, we characterize the interactions between the fimbrial adhesin FimH from uropathogenic *Escherichia coli* strains and its natural high-mannose type N-glycan binding epitopes on uroepithelial glycoproteins. Crystal structures and a detailed kinetic characterization of ligand-binding and dissociation revealed that the binding pocket of FimH evolved such that it recognizes the terminal α(1-2)-, α(1-3)- and α(1-6)-linked mannosides of natural high-mannose type N-glycans with similar affinity. We demonstrate that the 2,000-fold higher affinity of the domain-separated state of FimH compared to its domain-associated state is ligand-independent and consistent with a thermodynamic cycle in which ligand-binding shifts the association equilibrium between the FimH lectin and the FimH pilin domain. Moreover, we show that a single N-glycan can bind up to three molecules of FimH, albeit with negative cooperativity, so that a molar excess of accessible N-glycans over FimH on the cell surface favors monovalent FimH binding. Our data provide pivotal insights into the adhesion properties of uropathogenic *Escherichia coli* strains to their target receptors and a solid basis for the development of effective FimH antagonists.

Introduction

Multivalent carbohydrate-lectin interactions are fundamental for many biological processes, including cell-cell recognition, cell adhesion, signal transduction, immune system activation, and pathogen invasion.[1-2] A detailed molecular understanding of these interactions is therefore relevant for many medical applications.[3-8] Individual carbohydrate-lectin interactions typically show low affinities, with dissociation constants (K_d) in the micromolar to millimolar range.[8-10] However, the low affinities can be compensated by strong avidity effects that can dramatically improve pathogen adhesion. These avidity effects are caused by the presence of multiple lectins on the pathogen and multiple carbohydrate ligands on the target cell. A quantitative molecular description of multivalent host-pathogen interactions is usually hampered by the complexity of binding protein and target ligand distribution at the cell-cell interface.[11-12] Specifically, the precise, quantitative understanding of carbohydrate-lectin based host-pathogen interactions remains highly challenging.

Multivalent carbohydrate-lectin interactions play a key role in the bacterial adhesion and subsequent infection by pathogenic *Escherichia coli* (*E. coli*) strains, which are responsible for the vast majority of urinary tract infections (UTIs) in humans.[13] In the first critical infection step, the bacteria attach to the uroepithelium via filamentous type 1 pili, which are displayed on the bacterial surface in several hundred copies per cell.[14-15] Type 1 pili are composed of a 0.1 – 2 μm long, helical rod consisting of up to 3,000 copies of the pilus subunit FimA, and a tip fibrillum at the distal end formed by the pilus subunits FimF, FimG and FimH.[16] The adhesin FimH at the pilus tip is a lectin that recognizes terminal α-D-mannopyranosides of high-mannose type N-glycans on the surface of urothelial cells.[17] Due to its role as an essential virulence factor, FimH has attracted a lot of attention as a potential drug target for UTI treatment.[18-22]

FimH is a two-domain protein, composed of an N-terminal lectin domain ($FimH_L$) and a C-terminal pilin domain ($FimH_P$). $FimH_P$ connects FimH to the pilus and interacts with the

neighboring pilus subunit FimG via a mechanism termed donor strand complementation, in which the N-terminal extension of FimG (DsG) inserts as a β-strand into the immunoglobulin-like fold of $FimH_P$.[16] The two-domain architecture of FimH enables type 1 piliated *E. coli* cells to form "catch-bonds" after binding to target glycans: FimH shows the remarkable ability to bind ligands stronger under tensile mechanical forces acting on FimH·ligand complexes under the flow conditions of urine excretion, which prevents pathogen elimination by urination.[23] The catch-bonds formed by FimH are based on an allosteric mechanism in which the inter-domain interactions at the $FimH_P$-$FimH_L$ interface accelerate spontaneous ligand release from $FimH_L$ in the absence of mechanical force by 100,000-fold relative to the domain-separated FimH state induced by shear force. This results in a more than 1,000-fold weaker affinity of the domain-associated state of FimH (A-state) relative to the domain-separated S-state. The relatively weak affinity of FimH in the absence of shear force in turn favors bacterial motility along the urinary epithelium and invasion of new tissue areas.[24-25]

The catch-bond mechanism of FimH was established by characterizing the binding of the model ligand *n*-heptyl α-D-mannopyranoside (HM) to a soluble, monomeric version of full-length FimH, FimH·DsG, in which $FimH_P$ was stabilized with a synthetic peptide corresponding to DsG, and the isolated $FimH_L$ domain representing the S-state of FimH under shear force (Figure 1a).[26] Within the urinary tract environment, FimH recognizes a variety of glycoproteins, including uroplakin 1a, β1 and α3 integrins, and uromodulin.[17, 27-28] All these glycoproteins present high-mannose type N-glycans on their surface with glycoforms ranging from Man_5Gn_2 to Man_9Gn_2, and terminally exposed α-D-mannopyranosides that can be either α(1-2)-, α(1-3)- or α(1-6)-linked to the respective N-glycan (Figure 1b).[29-34] Notably, previous studies indicated that $FimH_L$ more readily binds to α(1-3)-linked versus α(1-2)-linked and α(1-6)-linked dimannosides.[35-36] However, fundamental questions on the interactions between FimH and its natural N-glycan binding epitopes remained unresolved: (i) How does FimH bind the

different terminal mannosides at the structural level? (ii) How do the different conformational states of FimH affect binding kinetics to their natural binding epitopes? (iii) How many FimH molecules can bind to a single high-mannose type N-glycan and is multivalent carbohydrate binding accompanied by steric hindrance effects or positive cooperativity?

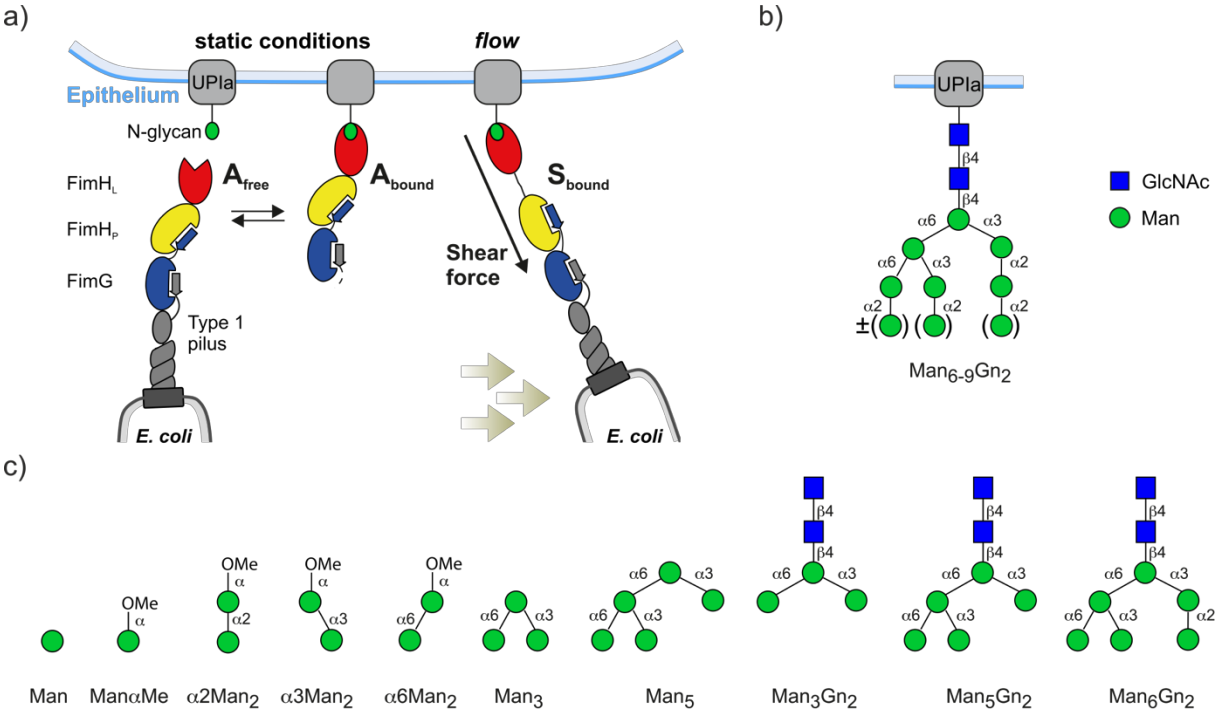

Figure 1. Catch-bond mechanism and binding epitopes of FimH-mediated adhesion. (a) Schematic representation of the FimH catch-bond mechanism. In absence of shear force, formation of the FimH-receptor interactions is characterized by a highly dynamic equilibrium between the A_{free} to the A_{bound} state, in which the $FimH_L$-$FimH_P$ domain interface remains intact. Fast binding and release to target receptors in the absence of shear forces are a prerequisite for bacterial motility in the urinary tract. Shear forces convert the A_{bound} to the domain-separated, high-affinity S_{bound} state, which shows the same binding properties as the isolated lectin domain $FimH_L$. The strongly increased affinity of S_{bound} prevents bacterial clearance by urine excretion. (b) The main FimH receptor in the urinary tract is uroplakin1a (UPIa) bearing high-mannose type N-glycans ranging from Man_6Gn_2 to Man_9Gn_2.[17] Terminal mannosides in these N-glycans can be α2-, α3- or α6-linked to the next mannopyranoside residue. c) Schematic representation of the mono- and multivalent ligands used in this study.

To address these questions, we used synthetic, α-linked mono- and dimannosides that represent natural terminal α-D-mannoside moieties present on FimH target glycoproteins in the bladder (Figure 1b,c). These monovalent model ligands enabled a complete kinetic and structural characterization of the binding properties for both the A- and S-state of FimH. The experiments revealed that FimH can bind multiple terminal N-glycan structures with similar affinity and demonstrate that the higher affinity of the S-state relative to the A-state is ligand-independent. High-resolution structures of multiple FimH·dimannoside complexes show that the flexibility of amino acid side chains of the extended FimH binding site supports binding to higher N-glycans. In addition, analytical size exclusion chromatography revealed that multiple copies of FimH can bind to a single high-mannose type N-glycan and allowed detailed, quantitative characterization of these multivalent carbohydrate-FimH interactions. This comparative analysis rationalizes the structural specificity of FimH to its natural ligands, and our results on the thermodynamics and kinetics of ligand-binding provide a framework for the development of efficient FimH antagonists.

Results & Discussion

Design and synthesis of the natural FimH model ligands

We previously analyzed the different functional and structural states of FimH with the model ligand HM.[26] Owing to its aliphatic *n*-heptyl substituent, HM binding properties may differ from high-mannose type N-glycans displayed on urothelial FimH target glycoproteins. To obtain a precise picture of FimH binding characteristics towards the different terminal mannopyranosides in natural N-glycans, we synthesized three natural model dimannosides, Manα(1-2)ManαMe (α2Man$_2$), Manα(1-3)ManαMe (α3Man$_2$) and Manα(1-6)ManαMe (α6Man$_2$) (Figure S1). The reducing end of each dimannoside ligand was modified by a methoxy group in the α-configuration, as in natural high-mannose type N-glycans. In addition, we included D-mannopyranose (Man) and methyl α-D-mannopyranoside (ManαMe) as reference ligands, allowing us to distinguish between contributions of the terminal and the subsequent mannopyranoside residue, as well as the effect of different glycosidic linkages on FimH binding (Figure 1b). To study multivalent carbohydrate-FimH interactions, FimH binding to the trimannoside (Man$_3$), the pentamannoside (Man$_5$), the core N-glycan Man$_3$Gn$_2$, Man$_5$Gn$_2$ and Man$_6$Gn$_2$ was analyzed (Figure 1c) (see below).

FimH binds α2-, α3- and α6-linked dimannosides with similar affinity

The K_d values for binding of the mono- and dimannoside ligands (Figure 1c) to FimH·DsG and FimH$_L$ were determined by equilibrium competition experiments using the fluorescein-labeled α-D-mannoside GN-FP as competitor.[26] GN-FP shows an about 2-fold fluorescence decrease and a strong fluorescence anisotropy increase at 528 nm upon binding to FimH. Its K_d values for binding to FimH·DsG and FimH$_L$ were determined to be 1.5×10^{-7} M and 7.0×10^{-11} M, respectively (Figure S2, Table 1).[26] Figure 2a,b shows the recorded equilibrium competition experiments in which GN-FP was displaced from FimH·DsG or FimH$_L$ with increasing

concentrations of the respective mannoside ligand. The deduced K_d values of Man, ManαMe, α2Man$_2$, α3Man$_2$ and α6Man$_2$ for binding to FimH·DsG and FimH$_L$ were in the range of 28 - 320 μM and 15 - 150 nM, respectively. Both FimH·DsG (A_{bound}) and FimH$_L$ (S_{bound}) showed highest affinity for α3Man$_2$, and 2-fold and 10-fold reduced affinity for α2Man$_2$ and α6Man$_2$, respectively (Table 1). In addition, α3Man$_2$ and α2Man$_2$ exhibited 4-fold and 10-fold higher affinities to both FimH states than the monosaccharides Man and ManαMe, indicating additional, stabilizing interactions between the subsequent mannopyranoside moieties of the di-mannosides and FimH (Table 1).

Stopped-flow tryptophan fluorescence kinetics revealed essentially identical association rates of ~ 2 - 3 x 10^5 $M^{-1}s^{-1}$ for all tested mono- and dimannoside ligands to the FimH A-state (FimH·DsG), demonstrating that the increased affinity to the A-state of the dimannosides relative to the monosaccharides originated from slower dissociation rates (Figure 2c and Table 1). This was confirmed by the kinetics of the GN-FP anisotropy increase during competitive ligand displacement by excess GN-FP (Figure 2d, Figure S3 and Table 1). Analogous results were obtained for ligand-binding to the FimH S-state (FimH$_L$): dimannosides were bound with higher affinity than monosaccharides, the order of affinity for the disaccharides remained α3Man$_2$ > α2Man$_2$ > α6Man$_2$, the on-rates of all mono- and dimannoside ligands were identical within a factor of two and differences in affinity were determined by the rates of spontaneous ligand dissociation (Figure 2b,d and Table 1).

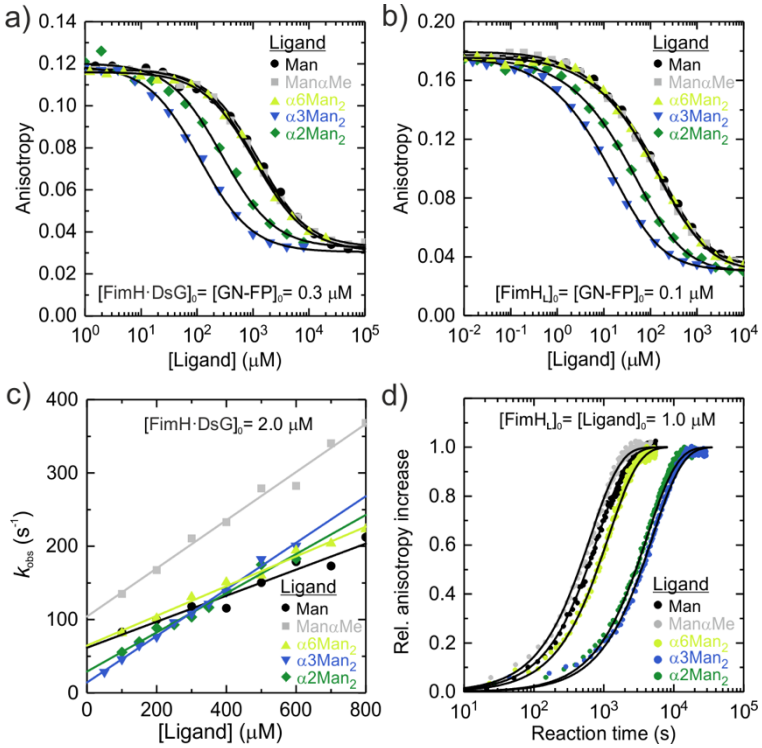

Figure 2. Thermodynamics and kinetics of ligand-binding and release by FimH·DsG (a,c) and FimH$_L$ (b,d) at pH 7.4 and 25°C. Ligand-binding equilibria of FimH·DsG (a) and FimH$_L$ (b), analyzed by competitive displacement of GN-FP via the increase in GN-FP fluorescence. The K_d values for GN-FP binding of 0.15 μM and 0.07 nM to FimH·DsG and FimH$_L$, respectively, were fixed during fitting the data globally (solid lines). (c) Stopped-flow kinetics of ligand-binding to FimH·DsG, recorded via the increase in tryptophan fluorescence above 320 nm. Kinetics were recorded under pseudo-first order conditions, and the observed pseudo-first order rate constants (k_{obs}) were plotted against ligand concentration. The slopes of the linear fits correspond to the respective second-order rate constants (k_{on}), and the y-axis intercepts correspond to the rates of spontaneous ligand dissociation (k_{off}). (d) Kinetics of spontaneous ligand dissociation from FimH$_L$, recorded via GN-FP binding after ligand dissociation. A solution with equimolar concentrations of FimH$_L$ and ligand (1 μM) was mixed with excess GN-FP (1.25 μM), and the increase in fluorescence anisotropy at 528±20 nm as a consequence of ligand dissociation and GN-FP binding was recorded. The obtained first-order kinetics (solid lines) were independent of GN-FP concentration (Figure S3) and thus directly monitored ligand dissociation.

Table 1. Kinetics and thermodynamics of ligand-binding to FimH·DsG and $FimH_L$.

Protein	Ligand	k_{on} ($M^{-1}s^{-1}$)	k_{off} (s^{-1})	k_{off}/k_{on} (kinetics; M)[a]	K_d (equilibrium; M)[b]
FimH·DsG (A-state)	Man	$(1.8\pm0.2) \times 10^{5}$	$(6.2\pm0.8) \times 10^{1}$	$(3.5\pm0.6) \times 10^{-4}$	$(3.2\pm0.2) \times 10^{-4}$
	ManαMe	$(3.3\pm0.2) \times 10^{5}$	$(1.0\pm0.1) \times 10^{2}$	$(3.2\pm0.3) \times 10^{-4}$	$(2.7\pm0.1) \times 10^{-4}$
	α6Man_2	$(2.0\pm0.1) \times 10^{5}$	$(6.5\pm0.5) \times 10^{1}$	$(3.2\pm0.3) \times 10^{-4}$	$(2.7\pm0.2) \times 10^{-4}$
	α2Man_2	$(2.7\pm0.1) \times 10^{5}$	$(2.9\pm0.5) \times 10^{1}$	$(1.1\pm0.2) \times 10^{-4}$	$(7.0\pm0.8) \times 10^{-5}$
	α3Man_2	$(3.2\pm0.1) \times 10^{5}$	$(1.4\pm0.3) \times 10^{1}$	$(4.4\pm0.9) \times 10^{-5}$	$(2.8\pm0.2) \times 10^{-5}$
	GN-FP	$(2.9\pm0.01) \times 10^{7}$	$(5.0\pm0.02) \times 10^{0}$	$(1.7\pm0.01) \times 10^{-7}$	$(1.5\pm0.1) \times 10^{-7}$ [c]
$FimH_L$ (S-state)	Man	$(8.4\pm0.3) \times 10^{3}$ [e]	$(1.2\pm0.003) \times 10^{-3}$	n.a.	$(1.5\pm0.1) \times 10^{-7}$
	ManαMe	$(1.3\pm0.1) \times 10^{4}$ [e]	$(1.6\pm0.01) \times 10^{-3}$	n.a.	$(1.2\pm0.05) \times 10^{-7}$
	α6Man_2	$(6.0\pm0.3) \times 10^{3}$ [e]	$(8.6\pm0.02) \times 10^{-4}$	n.a.	$(1.4\pm0.1) \times 10^{-7}$
	α2Man_2	$(5.5\pm0.3) \times 10^{3}$ [e]	$(2.4\pm0.01) \times 10^{-4}$	n.a.	$(4.4\pm0.2) \times 10^{-8}$
	α3Man_2	$(1.4\pm0.1) \times 10^{4}$ [e]	$(2.0\pm0.01) \times 10^{-4}$	n.a.	$(1.5\pm0.1) \times 10^{-8}$
	GN-FP	$(1.4\pm0.03) \times 10^{6}$ [e]	$(9.8\pm0.1) \times 10^{-5}$	n.a.	$(7.0\pm0.1) \times 10^{-11}$ [d]

Parameters were determined at pH 7.4 and 25°C. Errors are standard errors obtained from the respective fits. The rate constants k_{on} and k_{off} were determined from the experiments shown in Figure 2 and Figure S2. The K_d values for the complex formation between ligands and FimH·DsG and $FimH_L$ were (a) obtained from the ratio of rate constants (k_{off}/k_{on}), (b) calculated from the competition equilibria with GN-FP, (c) obtained from direct equilibrium titration experiments, or (d) were taken from reference 26, and (e) k_{on} values were calculated from K_d and k_{off}.

Table 2. Comparison of ligand-binding by FimH·DsG (A-state) versus $FimH_L$ (S-state).

Ligand	K_d (H·DsG)/ K_d (H_L)	k_{on} (H·DsG)/ k_{on} (H_L)	k_{off} (H·DsG)/ k_{off} (H_L)	$t_{1/2}$ (H·DsG) (ms)	$t_{1/2}$ (H_L) (min)
Man	2,100	21	52,000	11	10
ManαMe	2,300	25	63,000	7	7
α6Man_2	1,900	33	76,000	11	13
α2Man_2	1,600	49	121,000	24	48
α3Man_2	1,900	23	70,000	50	58
GN-FP	2,100	21	51,000	139	118

Values from Table 1 were used to calculate the respective ratios between the K_d, k_{on} and k_{off} values of FimH·DsG and $FimH_L$.

In summary, the results show that the FimH A-state (FimH·DsG) binds to all natural, terminal α-D-mannoside structures with medium affinity, while all D-mannosides are uniformly bound with approximately 2,000-fold higher affinity by the FimH S-state relative to the A-state. For each ligand, the higher affinity of the S-state results from an about 70,000-fold slower ligand dissociation from $FimH_L$ and an about 30-fold slower association compared to the A-state (Tables 1 and 2). The fact that the S-state shows a 2,000-fold higher affinity than the A-state independently of the respective ligand strongly indicates that the catch-bond mechanism of FimH is based on a thermodynamic cycle in which ligand-binding favors domain separation, as previously proposed.[37] The cycle predicts that the equilibrium constant of domain separation is shifted by a factor of 2,000 towards the S-state in the absence of mechanical force, i.e., the same factor by which the K_d values of the A-state are lower than those of the S-state (Figure 3). Despite the shift of the equilibrium from A_{bound} to S_{bound}, we could not detect the S_{bound} state in solution, because the kinetics of ligand-binding and dissociation for FimH·DsG did not deviate from those expected for binding to a single protein conformation (A-state) and reproduced the equilibrium K_d values within experimental error. Based on this, we estimate that S_{bound} was not populated by more than 10% in solution, and that the A_{free}/S_{free} equilibrium constant in the

absence of ligand is larger than 20,000 (Figure 3), in agreement with the observation that neither the S_{free} nor the S_{bound} state of FimH·DsG could be crystallized.[26, 38] The S_{bound} state of FimH mainly occurs under the shear forces during urine excretion, and the measured off-rates of the S_{bound} state define the lower limit of the off-rates under shear forces in the urethra.

Our thermodynamic cycle model is consistent with previous studies showing that monoclonal antibodies (mAbs) generated against $FimH_L$ (S-state) also improved ligand-binding of full-length FimH (A-state). Significant population of the S-state without shear stress was most likely observed because the S-state selective mAbs pulled the high-affinity S-state from the FimH A-state/S-state equilibrium.[25, 39] In summary, our results provide strong evidence that full-length FimH (FimH·DsG), and not $FimH_L$, is the best target for anti-adhesive drug screening, because the S_{free} state (represented by free $FimH_L$) is not significantly populated *in vivo* during colonization of the bladder habitat. We are fully convinced that the search for efficient FimH antagonists should primarily focus on molecules with high-affinity to and slow dissociation from the A-state of full-length FimH, since such drugs would be efficient anti-adhesives during early stages of infection. The fact that none of the FimH antagonists developed so far shows significantly lower off-rates than natural mannoside ligands indicates that there is still a large potential for developing efficient FimH antagonists.[40] The fluorescent mannoside GN-FP (Figure S2) should prove to be an excellent tool for thermodynamic and kinetic high-throughput screening of compound libraries for improved FimH antagonists (Figure S3).[41]

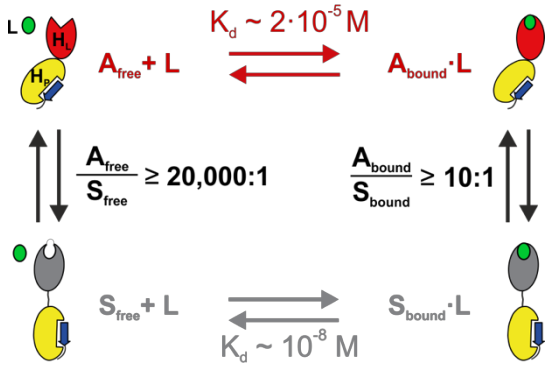

Figure 3. Thermodynamic cycle connecting the free energy of FimH domain-separation with the free energies of ligand-binding in solution. The A-state conformation of $FimH_L$ is colored red, while the S-state conformation of $FimH_L$ is colored grey. $FimH_P$, DsG, and the ligand (L) are colored yellow, blue and green, respectively. The lower limit of the A_{bound}/S_{bound} ratio of 10:1 corresponds to the estimated detection limit of a second, slow kinetic phase of ligand dissociation for FimH·DsG·ligand complexes in the absence of mechanical forces.

Structural analysis of FimH·oligomannoside complexes

We determined X-ray co-crystal structures of $FimH_L$ with the ligands $\alpha 2Man_2$, $\alpha 6Man_2$, and the trimannoside Man_3, as well as FimH·DsG bound to $\alpha 3Man_2$ and Man_3 with resolutions ranging from 1.72 to 2.50 Å (Figure S4 and Table S1). We compared them with the reported structures of $FimH_L$ with ManαMe (PDB ID: 5JCR) and Man_3Gn_2 (PDB ID: 2VCO).[42-43] In all FimH·DsG co-crystal structures, FimH adopts the domain-associated state, characterized by an intact domain interface (A_{bound} state) (Figure S4). All $FimH_L$ complex structures exhibit the elongated conformation of $FimH_L$ of the S_{bound} state, in agreement with the thermodynamic cycle model depicted in Figure 3.

Superposition of the binding sites of the five monovalent FimH·ligand complexes revealed a high structural similarity with a backbone r.m.s.d. of less than 0.3 Å (Figure 4 and Figure S5 – S8). Binding of the terminal α-D-mannopyranoside is identical in all FimH structures and is characterized by ten direct hydrogen bonds with the side chains of residues Asp54, Gln133, Asn135, Asp140 and to the main chain of Phe1 and Asp47. This extensive hydrogen bond

network is responsible for the specificity and high-affinity of FimH for all terminal α-D-mannopyranosides.[44]

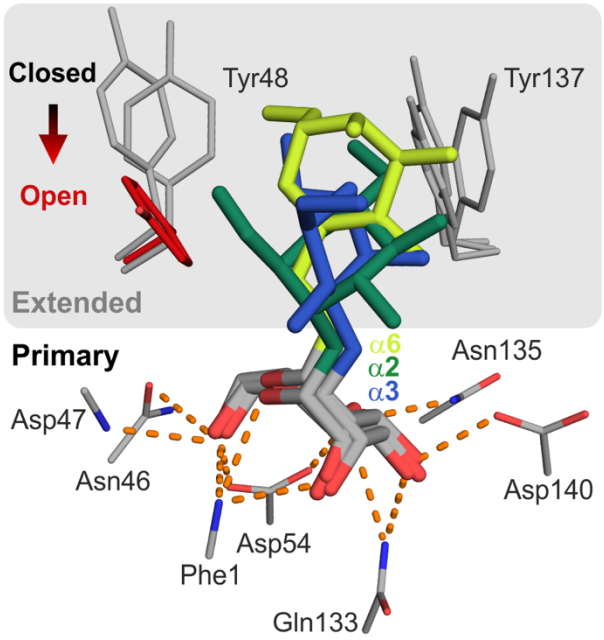

Figure 4. Ligand conformation in the FimH binding site of dimannoside complexes. The primary FimH binding site forms an extensive, conserved hydrogen bond network (orange) between the terminal α-D-mannopyranoside of all ligands (grey sticks with oxygen in red). The extended FimH binding site is mainly formed by the side chains of Tyr48 and Tyr137 that coordinate the subsequent mannoside residues and are colored green for α2-, blue for α3- and lime green for the α6-linked dimannosides. Tyr48 can adopt two side chain conformations, termed closed (grey, coordinating $\alpha2Man_2$ or $\alpha6Man_2$) and open (red, coordinating $\alpha3Man_2$) (see also Figure S5). The side chain flexibility of Tyr48 enables FimH to minimize steric hindrance effects, allowing FimH binding to multiple oligomannoside glycans.

The subsequent mannoside residues of the dimannoside ligands are mainly coordinated by the residues Tyr48, Ile52 and Tyr137 that line the entry of the primary binding site and are referred to as the "tyrosine gate" (Figure 4). The tyrosine gate can adopt a closed or an open conformation.[45-46] In the open conformation, the side chain of Tyr48 is rotated towards the mannose-binding pocket, while in the closed conformation the Tyr48 side chain points upwards to the distal end of the ligand-binding site (Figure 4 and Figure S5). In contrast to Tyr48, the

conformation of Tyr137 is unchanged in both conformations. Previously, chemical shift perturbation NMR experiments verified the existence of both Tyr48 side chain conformations in solution, but until now its biological function remained unclear.[45]

$FimH_L$ binds to the ligands Manα-Me, α2Man_2 and α6Man_2 with the tyrosine gate in the closed conformation, whereas in the $FimH_L$·Man_3Gn_2 and FimH·DsG·α3Man_2 complex the tyrosine gate is in the open conformation (Figure 4 and Figure S5-S7). In the dimannoside complexes, the subsequent α-methyl-mannosides show characteristic orientations of their α-methyl groups, which define the position of the next mannoside in natural N-glycans (Figure 4 and Figure S5). For the structure of the $FimH_L$·α6Man_2 complex, elongation by a third mannosyl residue in direction of the methoxy group would result in a clash with the closed gate conformation of the Tyr48 side chain (Figure 4 and Figure S6). However, a change of Tyr48 from closed to the open conformation would prevent this steric clash and enable FimH to bind the putative α(1-6) terminated N-glycan branch in a conformation that could be identical to the one obtained in our co-crystal structure (Figure S6). Therefore, we propose that the main function of the Tyr48 side chain flexibility is to support FimH binding to multiple high-mannose type N-glycans. This agrees with the $FimH_L$·Man_3Gn_2 complex structure, where the side chain conformation of Tyr48 was suggested to play an important role in ligand adaption of Man_3Gn_2 as a closed Tyr48 conformation would sterically clash with the first GalNAc of ligand Man_3Gn_2 (Figure S7). In addition, Wellens *et al.* showed that the apolar B-face of the subsequent mannoside residue of Man_3Gn_2 is involved in CH-π-stacking interactions with the aromatic side chain of Tyr48 in the open gate conformation (Figure S7).[42] Consequently, these interactions may stabilize not only the conformation of the subsequent mannoside, but also stabilize the open tyrosine gate conformation. Comparison of the FimH·DsG α3Man_2 and the $FimH_L$ Man_3Gn_2 co-crystal structures reveal identical orientations for the respective Manα(1-3)Man moieties and for the Tyr48 side chain (Figure S7). In natural high-mannose type N-glycans, the different subsequent

mannosides would, however, be α-linked to the rest of the N-glycan, in contrast to the β-linkage of Man_3Gn_2.

In addition to the monovalent FimH·dimannoside complexes, we determined the co-crystal structures of $FimH_L$ and FimH·DsG with the trimannoside ligand Man_3 (Figure 5 and Figure S4). In both structures, two FimH molecules were bound to a single Man_3 ligand (Man_3·$(FimH)_2$) and the $FimH_L$ domains showed clearly distinct relative orientations, respectively, stabilized by crystal contacts, demonstrating the Man_3 retained a high intrinsic structural flexibility when complexed with two FimH molecules (Figures 5 and S4).

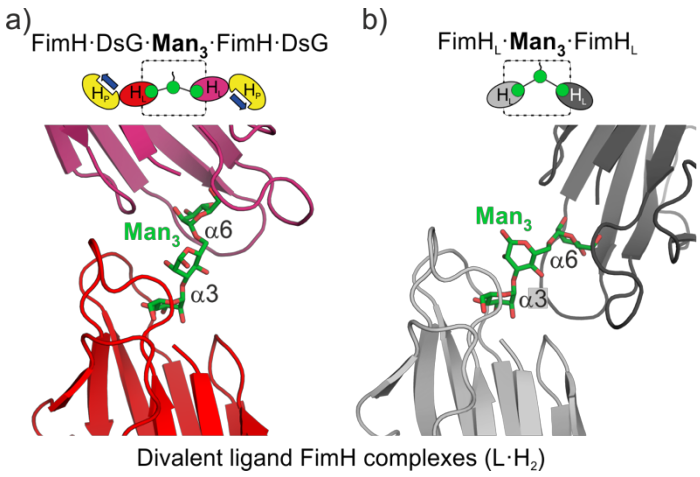

Figure 5. Cartoon representation of the Man_3·$(FimH·DsG)_2$ (a) and the Man_3·$(FimH_L)_2$ complex (b), demonstrating the high flexibility of Man_3 when complexed with two molecules of FimH. The FimH molecules bound to the terminal α3-linked mannopyranoside at the bottom of each panel are shown in the same orientation. Man_3 is shown in stick representation (green) with its oxygen atoms depicted in red.

Positive and negative cooperativity in multivalent oligomannoside-FimH interactions

The structures of the Man_3·$(FimH_L)_2$ complexes indicated that multivalent binding of FimH to natural high-mannose type N-glycans might also be formed when type 1 piliated *E. coli* cells interact with urinary endothelial cells. To test this possibility, we used the high-affinity variant $FimH_L$ and analyzed its binding stoichiometry to more complex oligomannosides by high-resolution analytical gel filtration. This allowed us to quantify free $FimH_L$, mono-, di- and trivalent oligomannoside complexes at equilibrium as a function of the respective

oligomannoside to $FimH_L$ ratio. We analyzed $FimH_L$ binding to five different oligomannoside ligands, Man_3, Man_5, Man_3Gn_2, Man_5Gn_2 and Man_6Gn_2 (Figure 6) and compared the equilibrium fractions of mono- and multivalent oligomannoside·$FimH_L$ complexes to those predicted for independent (non-cooperative) $FimH_L$ binding to the terminal mannopyranoside residues, assuming the same K_d values as those determined for $FimH_L$ binding to α6-, α3-, and α2Man_2 (Table 1) (Figure 6 and Figure S9). The results obtained for Man_3 (Figure 6e) confirmed the Man_3 : $FimH_L$ stoichiometry of 1 : 2 observed in the crystal structure (Figure 5b) and demonstrated positive cooperativity for $FimH_L$ binding, as the divalent Man_3·$(FimH_L)_2$ complex was strongly favored over the monovalent Man_3·$FimH_L$ complex at Man_3/$FimH_L$ ratios > 0.5 (Figure 6a,e). In contrast to Man_3, the divalent Man_3Gn_2·$(FimH_L)_2$ complex showed negative cooperativity, because the monovalent Man_3Gn_2·$FimH_L$ complex was significantly populated at Man_3Gn_2 : $FimH_L$ ratios < 0.5 and the fraction of $FimH_L$ in the divalent Man_3Gn_2·$(FimH_L)_2$ complex never exceeded 60% (Figure 6a,g). The results indicate that the β4-glycosidic linkage between the reducing end of Man_3 and the two N-acetylglucosamines in Man_3Gn_2 restricts the flexibility of the Man_3 unit and leads to steric clashes between both $FimH_L$ molecules in the Man_3Gn_2·$(FimH_L)_2$ complex. The negative cooperativity of $FimH_L$ binding to Man_3Gn_2 also agrees well with the finding that only one $FimH_L$ was bound to Man_3Gn_2 in the crystal structure of complex, namely to the α3-linked terminal mannopyranoside that is bound with higher affinity than the α6-linked mannopyranoside (Table 1, Figure S7).[42] Notably, analogous results were obtained for the potentially trivalent oligomannosides Man_5 and Man_5Gn_2, which both formed only divalent complexes with $FimH_L$ (Figure 6b,c,f,h). While two $FimH_L$ molecules bound independently (non-cooperatively) to Man_5, the two N-acetylglucosamines linked to the reducing end of the Man_5 unit again caused negative cooperativity in $FimH_L$ binding to Man_5Gn_2 (Figure 6b,c,f,h), identical to the negative cooperativity observed for Man_3Gn_2 (Figure 6g). The only oligomannoside ligand for which we could detect trivalent $FimH_L$ binding was Man_6Gn_2 (Figure 6i), but binding was again

accompanied by strong negative cooperativity. Compared to the predicted maximum fraction of 80% of $FimH_L$ in the trivalent $Man_6Gn_2 \cdot (FimH_L)_3$ complex at a $Man_6Gn_2/FimH_L$ ratio of 0.33 (Figure 6d), the fraction of $FimH_L$ in the trivalent complex never exceeded 20% (Figure 6d,i).

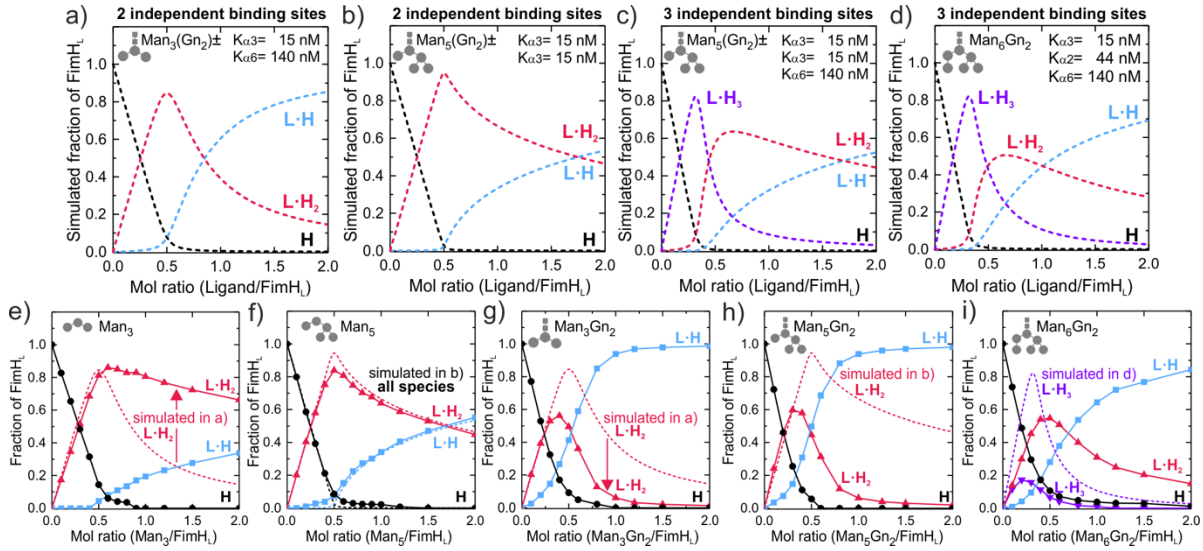

Figure 6. Binding of $FimH_L$ to multivalent oligomannoside ligands at pH 7.4 and 25°C, analyzed by analytical gel filtration. $FimH_L$ (constant concentration of 10 μM) was equilibrated with different amounts (0-20 μM) of the respective oligomannoside ligand. Free $FimH_L$ (H, black symbols) was then separated from monovalent ($L \cdot H$, blue symbols), divalent ($L \cdot H_2$, red symbols) and trivalent ($L \cdot H_3$, violet symbols) complexes by rapid gel filtration and the fraction of $FimH_L$ in the individual complexes was quantified by peak area integration (Figure S9).

(a-d) Predicted equilibrium fractions (dashed lines) of H, $L \cdot H$, $L \cdot H_2$ and $L \cdot H_3$ assuming i) independent $FimH_L$ binding to multivalent glycans, ii) K_d values of $FimH_L$ binding to terminal mannopyranoside residues identical to those determined for α6-, α3-, and α2Man_2 (Table 1) and iii) negligible complex dissociation during gel filtration. Simulations for two independent binding sites are shown for (a) Man_3Gn_2 or Man_3, (b) Man_5Gn_2 or Man_5, and for three independent binding sites for (c) Man_5Gn_2 or Man_5 and (d) Man_6Gn_2. (e-i) Measured fractions of $FimH_L$ in the complexes with the oligomannosides Man_3 (e), Man_5 (f), Man_3Gn_2 (g), Man_5Gn_2 (h) and Man_6Gn_2 (i). Data points are connected by solid lines. The predicted populations of the $L \cdot H_2$ and $L \cdot H_3$ species (dashed lines from a-d) were included in specific cases to illustrate deviations from non-cooperativity. The red arrows in (e) and (g) illustrate the positive cooperativity in binding of two $FimH_L$ molecules to Man_3 and the negative cooperativity in binding of two $FimH_L$ molecules to Man_3Gn_2.

Together, our results demonstrate for the first time that two or three copies of the type 1 pilus adhesin FimH are capable of binding to a single, natural high-mannose type N-glycan when FimH is present at excess over the target glycans. Inversely, monovalent FimH binding is favored when target glycans are present at excess over FimH, which is likely the case for the interactions between type 1 piliated *E. coli* and uroepithelial cells, because these cells are almost completely covered by a dense, two-dimensional surface layer of the FimH receptor uroplakin1a.[17, 47] However, multivalent interactions between a single glycan and multiple copies of FimH may occur *in vivo* during adhesion of type 1 piliated pathogens to other mammalian cells with low target glycan density, and could be facilitated by the intrinsic flexibility of the type 1 tip fibrillum.[48]

In all natural N-glycans investigated (Man_3Gn_2, Man_5Gn_2 and Man_6Gn_2), binding of more than one FimH molecule was accompanied with negative cooperativity, most likely due to steric clashes between the bound adhesins that are caused by a limited flexibility of the oligomannoside due to the β4-linkage of the proximal mannopyranoside with the two N-acetylglucosamines that is common to all natural N-glycans. The only case of positive cooperativity was observed for the non-natural ligand Man_3, possibly due to stabilizing interactions between the two bound FimH molecules. Thus, our results provide important information on the interplay between the density of available FimH target ligands on the urinary cell surface and the FimH/target ligand ratio.

Conclusions

Many pathogens, including type 1 piliated uropathogenic *E. coli*, make use of adhesins presented in a multivalent format on their cell surface for the attachment to target cells displaying multiple target ligands. Although full-length FimH at the fimbrial tip shows only moderate affinity ($3 \times 10^{-4} – 3 \times 10^{-5}$ M) for terminally exposed mannopyranosides displayed on high-mannose type N-glycans, up to 200 type 1 pili on a single *E. coli* cell enable stable

bacterial adhesion by simultaneously binding to surface glycans on the target cell. Our results show that individual FimH-glycan interactions are kinetically labile and only have very short lifetimes, in the range of 15 - 70 ms (Table 1). The highly dynamic FimH binding in the absence of shear forces prevents irreversible attachment of *E. coli* to its initial attachment site and favors bacterial motility on the urothelial surface, a prerequisite for the invasion of new tissue areas.[2, 49] In addition, these reversible multivalent interactions allow cell type-specific adhesion, because the target cells of the urinary epithelium show the highest density of FimH surface ligands.[50] Bacterial detachment from the urinary epithelium is only prevented under flow conditions during urine excretion when mechanical forces cause domain-separation in FimH and dramatically increase the lifetime of FimH·ligand complexes.

Notably, a natural, multivalent FimH antagonist exists, uromodulin, which has been proposed to compete with urinary epithelium cells for binding to type 1 piliated *E. coli*.[51] Uromodulin is the most abundant protein in human urine, bears high-mannose type N-glycans and polymerizes to more than 1 μm long, supramolecular filaments that may form multivalent complexes with type 1-piliated *E.coli* cells.[52] Consequently, multivalent, mannosylated compounds might be an alternative strategy for developing efficient anti-adhesives for UTI treatment.[53-57]

Our results clearly illustrate the need for developing FimH antagonists that dissociate more slowly from FimH than natural ligands, because monovalent FimH binders will only be able to competitively prevent FimH-mediated multivalent target cell adhesion if they show dramatically slower off-rates than FimH target glycans. All published high-affinity FimH antagonists, however, still show comparably fast dissociation from FimH (dissociation half-lives: 0.01 - 46 s), and their increased FimH affinity compared to natural glycans is due to faster association with FimH.[40] Notably, all fast-binding FimH antagonists possess aromatic substituents, indicating that π-stacking interactions with the tyrosine gate of FimH may lead to faster binding. This also agrees with our finding that our fluorescent mannoside, GN-FP, binds two orders of magnitude faster to FimH than all investigated dimannosides (Figure S2, Table 1).

GN-FP may become a very useful tool for high-throughput screening of compound libraries for slow dissociation from FimH with fluorescence anisotropy measurements (Figure 3d). The thermodynamic and kinetic data on the binding of natural ligands by FimH recorded in this study provides a solid framework for multivalent carbohydrate-lectin interactions and defines the requirements that need to be fulfilled by effective FimH antagonists for the treatment of urinary tract infections.

Author Information

Corresponding Author

*rudi@mol.biol.ethz.ch

Notes

The authors declare no competing financial interest.

Acknowledgments

We thank the staff at the Swiss Light Source (Villigen, Switzerland) for outstanding support for crystallographic data collection. This work was supported by the Swiss National Science Foundation (Projects 31003A_156304 and 310030B_176403 (R.G.)).

References

1. Fasting, C.; Schalley, C. A.; Weber, M.; Seitz, O.; Hecht, S.; Koksch, B.; Dernedde, J.; Graf, C.; Knapp, E. W.; Haag, R., Multivalency as a chemical organization and action principle. *Angew Chem Int Ed Engl* **2012,** *51*, 10472-98.
2. Kiessling, L. L.; Grim, J. C., Glycopolymer probes of signal transduction. *Chem Soc Rev* **2013,** *42*, 4476-91.
3. Bandlow, V.; Liese, S.; Lauster, D.; Ludwig, K.; Netz, R. R.; Herrmann, A.; Seitz, O., Spatial Screening of Hemagglutinin on Influenza A Virus Particles: Sialyl-LacNAc Displays on DNA and PEG Scaffolds Reveal the Requirements for Bivalency Enhanced Interactions with Weak Monovalent Binders. *J Am Chem Soc* **2017,** *139*, 16389-16397.
4. Munoz, A.; Sigwalt, D.; Illescas, B. M.; Luczkowiak, J.; Rodriguez-Perez, L.; Nierengarten, I.; Holler, M.; Remy, J. S.; Buffet, K.; Vincent, S. P.; Rojo, J.; Delgado, R.; Nierengarten, J. F.; Martin, N., Synthesis of giant globular multivalent glycofullerenes as potent inhibitors in a model of Ebola virus infection. *Nat Chem* **2016,** *8*, 50-7.
5. Qi, Z.; Bharate, P.; Lai, C. H.; Ziem, B.; Bottcher, C.; Schulz, A.; Beckert, F.; Hatting, B.; Mulhaupt, R.; Seeberger, P. H.; Haag, R., Multivalency at Interfaces: Supramolecular Carbohydrate-Functionalized Graphene Derivatives for Bacterial Capture, Release, and Disinfection. *Nano Lett* **2015,** *15*, 6051-7.
6. Weber, T.; Chandrasekaran, V.; Stamer, I.; Thygesen, M. B.; Terfort, A.; Lindhorst, T. K., Switching of bacterial adhesion to a glycosylated surface by reversible reorientation of the carbohydrate ligand. *Angew Chem Int Ed Engl* **2014,** *53*, 14583-6.
7. Mager, M. D.; LaPointe, V.; Stevens, M. M., Exploring and exploiting chemistry at the cell surface. *Nat Chem* **2011,** *3*, 582-9.
8. Bhatia, S.; Camacho, L. C.; Haag, R., Pathogen Inhibition by Multivalent Ligand Architectures. *J Am Chem Soc* **2016,** *138*, 8654-66.
9. Zhang, Y.; Li, Q.; Rodriguez, L. G.; Gildersleeve, J. C., An array-based method to identify multivalent inhibitors. *J Am Chem Soc* **2010,** *132*, 9653-62.
10. Dam, T. K.; Roy, R.; Das, S. K.; Oscarson, S.; Brewer, C. F., Binding of multivalent carbohydrates to concanavalin A and Dioclea grandiflora lectin. Thermodynamic analysis of the "multivalency effect". *J Biol Chem* **2000,** *275*, 14223-30.
11. Kitov, P. I.; Bundle, D. R., On the nature of the multivalency effect: a thermodynamic model. *J Am Chem Soc* **2003,** *125*, 16271-84.
12. Guo, Y.; Nehlmeier, I.; Poole, E.; Sakonsinsiri, C.; Hondow, N.; Brown, A.; Li, Q.; Li, S.; Whitworth, J.; Li, Z.; Yu, A.; Brydson, R.; Turnbull, W. B.; Pohlmann, S.; Zhou, D., Dissecting Multivalent Lectin-Carbohydrate Recognition Using Polyvalent Multifunctional Glycan-Quantum Dots. *J Am Chem Soc* **2017,** *139*, 11833-11844.
13. Ronald, A., The etiology of urinary tract infection: traditional and emerging pathogens. *The American journal of medicine* **2002,** *113 Suppl 1A*, 14S-19S.
14. Jones, C. H.; Pinkner, J. S.; Roth, R.; Heuser, J.; Nicholes, A. V.; Abraham, S. N.; Hultgren, S. J., FimH adhesin of type 1 pili is assembled into a fibrillar tip structure in the Enterobacteriaceae. *Proc Natl Acad Sci U S A* **1995,** *92*, 2081-5.
15. Hahn, E.; Wild, P.; Hermanns, U.; Sebbel, P.; Glockshuber, R.; Haner, M.; Taschner, N.; Burkhard, P.; Aebi, U.; Muller, S. A., Exploring the 3D molecular architecture of Escherichia coli type 1 pili. *J Mol Biol* **2002,** *323*, 845-57.
16. Waksman, G.; Hultgren, S. J., Structural biology of the chaperone-usher pathway of pilus biogenesis. *Nature reviews. Microbiology* **2009,** *7*, 765-74.
17. Zhou, G.; Mo, W. J.; Sebbel, P.; Min, G.; Neubert, T. A.; Glockshuber, R.; Wu, X. R.; Sun, T. T.; Kong, X. P., Uroplakin Ia is the urothelial receptor for uropathogenic Escherichia coli: evidence from in vitro FimH binding. *J Cell Sci* **2001,** *114*, 4095-103.

18. Flores-Mireles, A. L.; Walker, J. N.; Caparon, M.; Hultgren, S. J., Urinary tract infections: epidemiology, mechanisms of infection and treatment options. *Nature reviews. Microbiology* **2015,** *13*, 269-84.
19. Mydock-McGrane, L. K.; Hannan, T. J.; Janetka, J. W., Rational design strategies for FimH antagonists: new drugs on the horizon for urinary tract infection and Crohn's disease. *Expert Opin Drug Discov* **2017,** *12*, 711-731.
20. Ernst, B.; Magnani, J. L., From carbohydrate leads to glycomimetic drugs. *Nat Rev Drug Discov* **2009,** *8*, 661-77.
21. Terlizzi, M. E.; Gribaudo, G.; Maffei, M. E., UroPathogenic Escherichia coli (UPEC) Infections: Virulence Factors, Bladder Responses, Antibiotic, and Non-antibiotic Antimicrobial Strategies. *Front Microbiol* **2017,** *8*, 1566.
22. Klein, T.; Abgottspon, D.; Wittwer, M.; Rabbani, S.; Herold, J.; Jiang, X.; Kleeb, S.; Luthi, C.; Scharenberg, M.; Bezencon, J.; Gubler, E.; Pang, L.; Smiesko, M.; Cutting, B.; Schwardt, O.; Ernst, B., FimH antagonists for the oral treatment of urinary tract infections: from design and synthesis to in vitro and in vivo evaluation. *J Med Chem* **2010,** *53*, 8627-41.
23. Thomas, W. E.; Trintchina, E.; Forero, M.; Vogel, V.; Sokurenko, E. V., Bacterial adhesion to target cells enhanced by shear force. *Cell* **2002,** *109*, 913-23.
24. Aprikian, P.; Tchesnokova, V.; Kidd, B.; Yakovenko, O.; Yarov-Yarovoy, V.; Trinchina, E.; Vogel, V.; Thomas, W.; Sokurenko, E., Interdomain interaction in the FimH adhesin of Escherichia coli regulates the affinity to mannose. *J Biol Chem* **2007,** *282*, 23437-46.
25. Le Trong, I.; Aprikian, P.; Kidd, B. A.; Forero-Shelton, M.; Tchesnokova, V.; Rajagopal, P.; Rodriguez, V.; Interlandi, G.; Klevit, R.; Vogel, V.; Stenkamp, R. E.; Sokurenko, E. V.; Thomas, W. E., Structural basis for mechanical force regulation of the adhesin FimH via finger trap-like beta sheet twisting. *Cell* **2010,** *141*, 645-55.
26. Sauer, M. M.; Jakob, R. P.; Eras, J.; Baday, S.; Eris, D.; Navarra, G.; Berneche, S.; Ernst, B.; Maier, T.; Glockshuber, R., Catch-bond mechanism of the bacterial adhesin FimH. *Nat Commun* **2016,** *7*, 10738.
27. Eto, D. S.; Jones, T. A.; Sundsbak, J. L.; Mulvey, M. A., Integrin-mediated host cell invasion by type 1-piliated uropathogenic Escherichia coli. *PLoS Pathog* **2007,** *3*, e100.
28. Akiyoshi, B.; Sarangapani, K. K.; Powers, A. F.; Nelson, C. R.; Reichow, S. L.; Arellano-Santoyo, H.; Gonen, T.; Ranish, J. A.; Asbury, C. L.; Biggins, S., Tension directly stabilizes reconstituted kinetochore-microtubule attachments. *Nature* **2010,** *468*, 576-9.
29. Xie, B.; Zhou, G.; Chan, S. Y.; Shapiro, E.; Kong, X. P.; Wu, X. R.; Sun, T. T.; Costello, C. E., Distinct glycan structures of uroplakins Ia and Ib: structural basis for the selective binding of FimH adhesin to uroplakin Ia. *J Biol Chem* **2006,** *281*, 14644-53.
30. Litynska, A.; Pochec, E.; Hoja-Lukowicz, D.; Kremser, E.; Laidler, P.; Amoresano, A.; Monti, C., The structure of the oligosaccharides of alpha3beta1 integrin from human ureter epithelium (HCV29) cell line. *Acta Biochim Pol* **2002,** *49*, 491-500.
31. Litynska, A.; Przybylo, M.; Ksiazek, D.; Laidler, P., Differences of alpha3beta1 integrin glycans from different human bladder cell lines. *Acta Biochim Pol* **2000,** *47*, 427-34.
32. Serafini-Cessi, F.; Dall'Olio, F.; Malagolini, N., High-mannose oligosaccharides from human Tamm-Horsfall glycoprotein. *Biosci Rep* **1984,** *4*, 269-74.
33. Dall'Olio, F.; de Kanter, F. J.; van den Eijnden, D. H.; Serafini-Cessi, F., Structural analysis of the preponderant high-mannose oligosaccharide of human Tamm-Horsfall glycoprotein. *Carbohydr Res* **1988,** *178*, 327-32.
34. van Rooijen, J. J.; Voskamp, A. F.; Kamerling, J. P.; Vliegenthart, J. F., Glycosylation sites and site-specific glycosylation in human Tamm-Horsfall glycoprotein. *Glycobiology* **1999,** *9*, 21-30.
35. Bouckaert, J.; Mackenzie, J.; de Paz, J. L.; Chipwaza, B.; Choudhury, D.; Zavialov, A.; Mannerstedt, K.; Anderson, J.; Pierard, D.; Wyns, L.; Seeberger, P. H.; Oscarson, S.; De Greve,

H.; Knight, S. D., The affinity of the FimH fimbrial adhesin is receptor-driven and quasi-independent of Escherichia coli pathotypes. *Mol Microbiol* **2006,** *61*, 1556-68.
36. Dumych, T.; Bridot, C.; Gouin, S. G.; Lensink, M. F.; Paryzhak, S.; Szunerits, S.; Blossey, R.; Bilyy, R.; Bouckaert, J.; Krammer, E. M., A Novel Integrated Way for Deciphering the Glycan Code for the FimH Lectin. *Molecules* **2018,** *23*.
37. Yakovenko, O.; Tchesnokova, V.; Sokurenko, E. V.; Thomas, W. E., Inactive conformation enhances binding function in physiological conditions. *Proc Natl Acad Sci U S A* **2015,** *112*, 9884-9.
38. Kalas, V.; Pinkner, J. S.; Hannan, T. J.; Hibbing, M. E.; Dodson, K. W.; Holehouse, A. S.; Zhang, H.; Tolia, N. H.; Gross, M. L.; Pappu, R. V.; Janetka, J.; Hultgren, S. J., Evolutionary fine-tuning of conformational ensembles in FimH during host-pathogen interactions. *Sci Adv* **2017,** *3*, e1601944.
39. Tchesnokova, V.; Aprikian, P.; Kisiela, D.; Gowey, S.; Korotkova, N.; Thomas, W.; Sokurenko, E., Type 1 fimbrial adhesin FimH elicits an immune response that enhances cell adhesion of Escherichia coli. *Infect Immun* **2011,** *79*, 3895-904.
40. Frei, P.; Pang, L.; Silbermann, M.; Eris, D.; Muhlethaler, T.; Schwardt, O.; Ernst, B., Target-directed Dynamic Combinatorial Chemistry: A Study on Potentials and Pitfalls as Exemplified on a Bacterial Target. *Chemistry* **2017,** *23*, 11570-11577.
41. Mayer, K.; Eris, D.; Schwardt, O.; Sager, C. P.; Rabbani, S.; Kleeb, S.; Ernst, B., Urinary Tract Infection: Which Conformation of the Bacterial Lectin FimH Is Therapeutically Relevant? *J Med Chem* **2017,** *60*, 5646-5662.
42. Wellens, A.; Garofalo, C.; Nguyen, H.; Van Gerven, N.; Slattegard, R.; Hernalsteens, J. P.; Wyns, L.; Oscarson, S.; De Greve, H.; Hultgren, S.; Bouckaert, J., Intervening with urinary tract infections using anti-adhesives based on the crystal structure of the FimH-oligomannose-3 complex. *PLoS One* **2008,** *3*, e2040.
43. Rabbani, S.; Fiege, B.; Eris, D.; Silbermann, M.; Jakob, R. P.; Navarra, G.; Maier, T.; Ernst, B., Conformational switch of the bacterial adhesin FimH in the absence of the regulatory domain: Engineering a minimalistic allosteric system. *J Biol Chem* **2018,** *293*, 1835-1849.
44. Bouckaert, J.; Berglund, J.; Schembri, M.; De Genst, E.; Cools, L.; Wuhrer, M.; Hung, C. S.; Pinkner, J.; Slattegard, R.; Zavialov, A.; Choudhury, D.; Langermann, S.; Hultgren, S. J.; Wyns, L.; Klemm, P.; Oscarson, S.; Knight, S. D.; De Greve, H., Receptor binding studies disclose a novel class of high-affinity inhibitors of the Escherichia coli FimH adhesin. *Mol Microbiol* **2005,** *55*, 441-55.
45. Fiege, B.; Rabbani, S.; Preston, R. C.; Jakob, R. P.; Zihlmann, P.; Schwardt, O.; Jiang, X.; Maier, T.; Ernst, B., The tyrosine gate of the bacterial lectin FimH: a conformational analysis by NMR spectroscopy and X-ray crystallography. *Chembiochem* **2015,** *16*, 1235-46.
46. Han, Z.; Pinkner, J. S.; Ford, B.; Obermann, R.; Nolan, W.; Wildman, S. A.; Hobbs, D.; Ellenberger, T.; Cusumano, C. K.; Hultgren, S. J.; Janetka, J. W., Structure-based drug design and optimization of mannoside bacterial FimH antagonists. *J Med Chem* **2010,** *53*, 4779-92.
47. Min, G.; Wang, H.; Sun, T. T.; Kong, X. P., Structural basis for tetraspanin functions as revealed by the cryo-EM structure of uroplakin complexes at 6-A resolution. *J Cell Biol* **2006,** *173*, 975-83.
48. Gossert, A. D.; Bettendorff, P.; Puorger, C.; Vetsch, M.; Herrmann, T.; Glockshuber, R.; Wuthrich, K., NMR structure of the Escherichia coli type 1 pilus subunit FimF and its interactions with other pilus subunits. *J Mol Biol* **2008,** *375*, 752-63.
49. Weis, W. I.; Drickamer, K., Structural basis of lectin-carbohydrate recognition. *Annu Rev Biochem* **1996,** *65*, 441-73.
50. Rao, J.; Lahiri, J.; Isaacs, L.; Weis, R. M.; Whitesides, G. M., A trivalent system from vancomycin.D-ala-D-Ala with higher affinity than avidin.biotin. *Science* **1998,** *280*, 708-11.

51. Pak, J.; Pu, Y.; Zhang, Z. T.; Hasty, D. L.; Wu, X. R., Tamm-Horsfall protein binds to type 1 fimbriated Escherichia coli and prevents E. coli from binding to uroplakin Ia and Ib receptors. *J Biol Chem* **2001,** *276*, 9924-30.
52. Devuyst, O.; Olinger, E.; Rampoldi, L., Uromodulin: from physiology to rare and complex kidney disorders. *Nat Rev Nephrol* **2017,** *13*, 525-544.
53. Lee, D. W.; Kim, T.; Park, I. S.; Huang, Z.; Lee, M., Multivalent nanofibers of a controlled length: regulation of bacterial cell agglutination. *J Am Chem Soc* **2012,** *134*, 14722-5.
54. Sattigeri, J. A.; Garg, M.; Bhateja, P.; Soni, A.; Rauf, A. R. A.; Gupta, M.; Deshmukh, M. S.; Jain, T.; Alekar, N.; Barman, T. K.; Jha, P.; Chaira, T.; Bambal, R. B.; Upadhyay, D. J.; Nishi, T., Synthesis and evaluation of thiomannosides, potent and orally active FimH inhibitors. *Bioorg Med Chem Lett* **2018,** *28*, 2993-2997.
55. Tsakama, M.; Ma, X.; He, Y.; Chen, W.; Dai, X., A Simple Mannose-Coated Poly (p-Phenylene Ethynylene) for Qualitative Bacterial Capturing. *Molecules* **2018,** *23*.
56. Mousavifar, L.; Touaibia, M.; Roy, R., Development of Mannopyranoside Therapeutics against Adherent-Invasive Escherichia coli Infections. *Acc Chem Res* **2018**.
57. Nagahori, N.; Lee, R. T.; Nishimura, S.; Page, D.; Roy, R.; Lee, Y. C., Inhibition of adhesion of type 1 fimbriated Escherichia coli to highly mannosylated ligands. *Chembiochem* **2002,** *3*, 836-44.

TOC GRAPHIC